PHYSICAL REVIEW B **84**, 054423 (2011)

Analysis of the line shape of electrically detected ferromagnetic resonance

M. Harder,[1] Z. X. Cao,[1,2] Y. S. Gui,[1] X. L. Fan,[1,3] and C.-M. Hu[1,*]

[1]*Department of Physics and Astronomy, University of Manitoba, Winnipeg, Canada R3T 2N2*

[2]*National Lab for Infrared Physics, Shanghai Institute of Technical Physics, Chinese Academy of Science, Shanghai 200083, People's Republic of China*

[3]*The Key Lab for Magnetism and Magnetic Materials of Ministry of Education, Lanzhou University, Lanzhou 730000, People's Republic of China*

(Received 9 May 2011; revised manuscript received 30 June 2011; published 8 August 2011)

This work reviews and examines two particular issues related with the new technique of electrical detection of ferromagnetic resonance (FMR). This powerful technique has been broadly applied for studying magnetization and spin dynamics over the past ten years. The first issue is the relation and distinction between different mechanisms that give rise to a photovoltage via FMR in spintronic devices, and the second is the proper analysis of the FMR line shape, which has become the "Achilles heel" in interpreting experimental results, especially for either studying the spin pumping effect or quantifying spin Hall angles via the electrically detected FMR.

DOI: 10.1103/PhysRevB.84.054423 PACS number(s): 85.75.−d, 75.40.Gb, 76.50.+g, 42.65.−k

I. INTRODUCTION

Electrical detection of ferromagnetic resonance (FMR) in ferromagnets (FM) is a powerful new experimental tool which has transformed the research on spin and magnetization dynamics.[1–32] Over the past ten years, this technique has generated a great deal of interest in the communities of magnetism, spintronics, and microwave technologies. It has been broadly applied for studying diverse material structures, ranging from ferromagnetic thin films such as Py (permalloy, $Ni_{80}Fe_{20}$),[3,6,11,13], CrO_2,[14] Fe_3O_4,[14] single crystal Fe,[16] GaMnAs,[17] and $La_{1-x}Sr_xMnO_3$,[18] bilayer devices such as Py/Pt,[7,8,19,20,24,25] Py/Au,[19,20] Py/GaAs,[21] and $Y_3Fe_5O_{12}$/Pt,[22,23] to a variety of magnetic tunneling junctions (MTJ) based on magnetic multilayers.[4,9,10,15] From a technical standpoint, its high sensitivity has made it possible to quantitatively determine spin boundary conditions[26] and to directly measure nonlinear magnetization damping,[27–29] the quasiparticle mass for the domain wall,[30] the phase diagram of the spin-transfer driven dynamics[2] and various kinds of parametric spin wave excitations.[2,31,32] Its capability to probe the interplay of spins, charges, and photons has been utilized for studying spin rectification,[11,12] spin pumping,[7] spin torque,[15] and spin Hall effects,[19,24,25] which have led to the proposing and realization of novel dynamic spintronic devices such as the spin battery,[7,33–36] spin diode,[4,10,15] spin dynamo,[11,12] and spin demodulator.[37] Very recently, its ability to detect coherent processes[38–40] has enabled electrical probing of the spin-resonance phase and the relative phase of electromagnetic waves,[38] which pave new ways for microwave sensing,[41] nondestructive imaging,[38] and dielectric spectroscopy.[39] Such a coherent capability is especially exciting as it resembles the latest achievement in semiconductor spintronics, where a new platform for coherent optical control of spin/charge currents has been developed by using nonresonant quantum interferences.[42–44]

From the physical standpoint, many different effects may generate a time-independent dc voltage in magnetic materials via the FMR. Reported mechanisms involve spin rectification,[11,12] spin pumping,[7] spin torque,[15] spin diode,[4,10,15] spin Hall,[24] and inverse spin Hall effects.[8,19,20,25] Two major issues stand out here. (1) A unified picture clarifying the relations and distinctions between such diverse mechanisms has not been established, which leads to increasing controversy and confusion in interpreting and understanding experimental results. A stunning example of this issue is found in the very recent studies of the spin Hall effect via electrically detected FMR, where two similar experiments[19,24] performed on similar devices were interpreted completely differently.[45] (2) When more than one mechanism simultaneously plays a role in the FMR generated dc voltage, proper interpretation requires a quantitative analysis of the FMR line shape. In our opinion, such a seemingly trivial issue has become the "Achilles heel" of this powerful experimental technique, especially in recent studies of spin pumping and the spin Hall effect via electrically detected FMR. The purpose of this article is to address these two critical issues with a brief review of the key physics of this subject, followed by systematically measured experimental data with detailed theoretical analysis.

This paper is split into three main sections. First we provide a brief review of different mechanisms which may generate the photovoltage via the FMR. Then we use the dynamic susceptibility obtained from a solution of the Landau-Lifshitz-Gilbert equation to derive analytical formulas for analyzing the line shape and the symmetry properties of the photovoltage generated through spin rectification. Finally we present experimental results measured from different samples, at different frequencies, and in different experimental configurations, showing that the FMR line shape is determined by the relative phase of microwaves which is sample and frequency dependent.

II. A BRIEF REVIEW OF ELECTRICAL DETECTION OF FMR

Under microwave excitation at angular frequency ω, the rf electric ($\mathbf{e}$) and magnetic ($\mathbf{h}$) fields inside a ferromagnetic material can be described as $\mathbf{e} = \mathbf{e}_0 e^{-i\omega t}$ and $\mathbf{h} = \mathbf{h}_0 e^{-i(\omega t - \Phi)}$, respectively. Note that in general, due to the inevitable losses of microwaves propagating inside the ferromagnetic material,

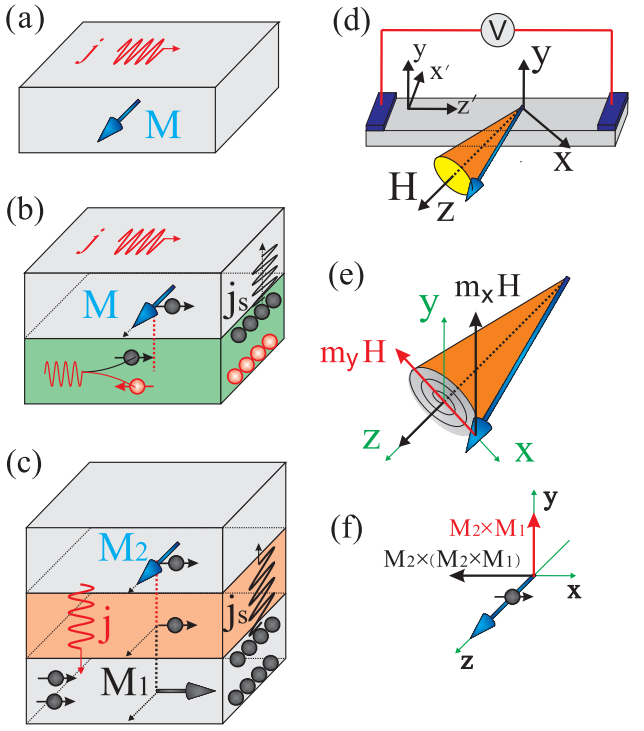

FIG. 1. (Color online) Dynamic response of magnetic structures under microwave irradiation: (a) Single thin film layer where the spin rectification is due to the magnetic field torque as shown in (e). (b) Magnetic bilayer device which has two rf currents $\mathbf{j}$ and $\mathbf{j}_s$ with different spin polarizations. Therefore spin rectification is due to both magnetic field and spin torques. (c) Magnetic tunneling junction with both $\mathbf{j}$ and $\mathbf{j}_s$. (d) Coordinate system for single ferromagnetic microstrips measured in this work under an in-plane applied static magnetic field $\mathbf{H}$. The z' axis is fixed along the strip and the direction of current flow, while the z axis is rotated to follow the direction of $\mathbf{H}$. (e) Components of magnetic field torque. (f) Spin torque in magnetic tunneling junction.

there is a phase difference Φ between the dynamic $\mathbf{e}$ and $\mathbf{h}$ fields. Such a relative phase is determined by the frequency-dependent wave impedance of the materials.[46] As shown in Fig. 1, the rf $\mathbf{e}$ field drives a rf current $\mathbf{j} = \sigma\mathbf{e}$, while the rf $\mathbf{h}$ field exerts a field torque on the magnetization and drives it to precess around its equilibrium direction [Fig. 1(e)]. Such a magnetization precession is described by the nonequilibrium magnetization $\mathbf{m} = \hat{\chi}\mathbf{h}$. Here σ and $\hat{\chi}$ are the high-frequency conductivity and Polder tensor, respectively. Note that due to the resonance nature of the precession, $\mathbf{m}$ lags $\mathbf{h}$ by a spin resonance phase Θ. However, despite the phase of Φ and Θ, the dynamic $\mathbf{j}$ and $\mathbf{m}$ keep the coherence of their respective driving fields, so that the product of any combination of their components may generate a time-independent signal proportional to $\langle \mathrm{Re}(\tilde{j}) \cdot \mathrm{Re}(\tilde{m}) \rangle$, where $\langle\ \rangle$ denotes the time average. The amplitude of such a signal depends on the phase difference of $\mathbf{j}$ and $\mathbf{m}$, which can be easily understood from the trigonometric relation $\langle \cos(\omega t) \cdot \cos(\omega t - \Phi) \rangle = \cos(\Phi)/2$. This is the spin rectification[11] as we highlight in Table I. For transport measurements on magnetic structures under microwave irradiation, various magnetoresistance effects such as anisotropic magnetoresistance (AMR), giant magnetoresistance (GMR), and tunneling magnetoresistance (TMR) make nonlinear corrections to Ohm's law via their corresponding magnetoresistance terms,[12] which typically lead to the product of $\mathbf{j}$ and $\mathbf{m}$. Such h-field torque induced spin rectifications are listed in Table I by the terms labeled V_{SR}^{h}. The earliest report on the measurement of V_{SR}^{h} dates to Juretschke's pioneering paper[47] published in 1960, although the power sensitivity achieved at that time was too small to be practically used (it was about 3 orders of magnitude smaller than that found in Ref. 11). The general feature of V_{SR}^{h} is that its amplitude depends on both the relative phase Φ and the spin resonance phase Θ, which leads to a characteristic phase signature of the FMR line shape.[38,39]

Similar to the effect of the rf $\mathbf{h}$ field torque, a spin torque induced by a spin polarized current may also drive magnetization precession. For example, in a bilayer [Fig. 1(b)] made of a ferromagnetic layer and a nonmagnetic layer with spin-orbit coupling,[24] in addition to the rf current $\mathbf{j}$ flowing in the ferromagnetic layer, the rf $\mathbf{e}$ field also induces a rf charge current flowing in the nonmagnetic layer. Via the spin Hall effect in such a nonmagnetic layer with spin-orbit coupling, the rf charge current can be converted into a spin current $\mathbf{j}_s$, which may flow into the ferromagnetic layer and then drive the magnetization precession via the spin torque. Such a spin torque induced nonequilibrium magnetization can be described by $\mathbf{m} = \hat{\chi}_j \mathbf{j}_s$, where the spin-torque susceptibility tensor $\hat{\chi}_j$ introduces a spin resonance phase ϑ that is different from Θ in $\hat{\chi}$. Following a similar consideration for the h-field induced spin rectification, a photovoltage depending on the spin torque may be generated in the ferromagnetic layer. This is the physical origin of the spin torque induced spin rectification effect,[24] which is listed in Table I by the term labeled V_{SR}^{s}. In MTJ [Fig. 1(c)], the spin polarized current $\mathbf{j}_s$ can be directly generated in the ferromagnetic layer where the magnetization is pinned along a different direction than that of the free layer. It tunnels into the free layer and drives the magnetization precession via the spin torque [Fig. 1(f)]. The spin torque induced spin rectification signal in MTJ has been measured in spin diodes,[4,10,15] which is also listed in Table I by the term labeled V_{SR}^{s}.

Over the past few years, systematic studies on spin rectifications induced by the h-field torque (V_{SR}^{h}) and spin torque (V_{SR}^{s}) have been performed, respectively, at the University of Manitoba[11,12,16,17,26–28,38,39,41] and Cornell University.[2,9,15,24,50] It has been found that due to the coherent nature of spin rectification, both V_{SR}^{h} and V_{SR}^{s} depend on the phase difference between $\mathbf{j}$ and $\mathbf{m}$. However, only the field torque spin rectification (V_{SR}^{h}) can be controlled by the relative phase Φ of the microwaves.[38]

In addition to such coherent spin rectification effects, it is known that at the interface between a ferromagnetic and a nonmagnetic layer, microwave excitation may generate a spin polarized current flowing across the interface via the spin pumping effect.[33] This effect has been observed in a few striking experiments by measuring either transmission electron spin resonance[48] or enhanced magnetization damping.[49] It involves FMR, exchange coupling, and nonequilibrium spin diffusion. An intuitive physical picture of spin pumping was given by the classical paper of Silsbee *et al.*[48] published in 1979, which used a phenomenological model to highlight the key mechanism of dynamic exchange coupling between

the precessing magnetization and the spin polarized current. Such a dynamic coupling significantly "amplifies" the effect of the rf **h** field in generating nonequilibrium spins, which diffuse across the ferromagnetic (FM) /normal metal (NM) interface to form the spin polarized current. Microscopically, spin pumping is a consequence of spin dependent reflectivity and transmission parameters of NM electrons at the FM/NM interface. Spin mixing conductance is the main parameter driving spin pumping, which was rigorously derived by Tserkovnyak *et al*.[33] Theoretical derivation is not trivial but the picture behind it is very clear and using magnetoelectronics Kirchhoff's laws[33] one can easily apply such a derivation to different dynamical configurations. It has been proposed that the spin current generated via spin pumping may also induce a photovoltage, either across the interface in a spin battery,[7,34–36] or within the nonmagnetic layer via the inverse spin Hall effect.[8,19,20,25] Recent experiments performed on magnetic bilayers[24] have suggested that spin-pumping induced dc voltage (the term V_{SP} in Table I) is about two orders of magnitude smaller than spin torque induced spin rectification (the term labeled V^{s}_{SR}). In contrast to phase sensitive coherent spin rectification effects, the proposed spin-pumping photovoltage is based on incoherent spin diffusion and FMR absorption. Hence, the anticipated FMR line shape of V_{SP} is symmetric and phase independent.

From the above discussion, it is clear that the line shape analysis plays the essential role in distinguishing the microwave photovoltage generated by different mechanisms. This issue has been partially addressed by a number of theoretical[50,51] and experimental works[4,10,15] studying nanostructured MTJs where the photovoltage is dominated by the spin torque induced spin rectification. Enlightened by these works and also based on our own previous studies,[12,38] we discuss in the following the critical issue of FMR line shape analysis in microstructured devices, where the field and spin torque induced spin rectification may have comparable strength. Our theoretical consideration and experimental data demonstrate the pivotal role of the relative phase Φ, which was often underestimated in previous studies. Via systematic studies with different device structures, measurement configurations and frequency ranges, we find that Φ has to be calibrated at different microwave frequencies for each device independently. Hence our results are in strong contradiction with the recent experiment performed on microstructured magnetic bilayers for quantifying the spin Hall angles, where Φ was set to zero for all devices at all microwave frequencies[19,20] based on the results of line shape analysis performed on reference samples.[52]

III. FMR LINE SHAPE

A. The characteristic signature

From Table I the role of the phase in the FMR line shape symmetry can be understood by considering the spin rectified voltage $V \propto \langle \mathrm{Re}(\tilde{j}) \cdot \mathrm{Re}(\tilde{m}) \rangle$. For spin rectification induced by the field torque, depending on the experimental configuration, at least one matrix component χ of the Polder tensor $\widehat{\chi}$ will drive the FMR; whether an on or off-diagonal component is responsible for the magnetization precession depends on the measurement configuration. Since $\mathbf{m} = \widehat{\chi}\mathbf{h}$, $\mathrm{Re}(\tilde{m}) \propto \mathrm{Re}(\chi)\cos(\omega t - \Phi) + \mathrm{Im}(\chi)\sin(\omega t - \Phi)$. Therefore after time averaging a time independent dc voltage is found $V(\Phi) \propto [\mathrm{Re}(\chi)\cos(\Phi) - \mathrm{Im}(\chi)\sin(\Phi)]$. It is well known that for diagonal matrix elements, $\mathrm{Re}(\chi)$ has a dispersive line shape while $\mathrm{Im}(\chi)$ has a symmetric line shape. However, since the on- and off-diagonal susceptibilities differ by a phase of 90°, if the FMR is driven by an off-diagonal susceptibility, the roles are reversed and $\mathrm{Re}(\chi)$ has a symmetric line shape while $\mathrm{Im}(\chi)$ has a dispersive line shape.

Based on the simple argument leading to the above $V(\Phi)$ expression, one can see that the line shape symmetry has a characteristic dependence on the relative phase Φ between electric and magnetic fields. Thus when measuring FMR based on the field torque induced spin rectification effect, it is important to consider the relative phase, whereas for a spin pumping measurement which measures $|\mathbf{m}|^2$, or for a spin torque induced spin rectification which involves $|\mathbf{j}|^2$, the relative phase does not influence the experiment. In the next two sections, a detailed analysis is given by solving the Landau-Lifshitz-Gilbert equation, which leads to analytical formulas describing the symmetric and dispersive line shapes for different measurement configurations.

B. The dynamic susceptibility

The Landau-Lifshitz-Gilbert equation provides a phenomenological description of ferromagnetic dynamics based

TABLE I. Relation and distinctions between different mechanisms for microwave photovoltages induced by FMR. (For simplicity we consider only one matrix element of $\hat{\chi}$ and $\hat{\chi}_j$ which is responsible for the spin rectification. $\tilde{j}$ and $\tilde{m}$ denote a corresponding component of the time-dependent current and magnetization, respectively.)

rf driving Effect	$\tilde{e} = e_0 e^{-i\omega t}$ Ohm's law	$\tilde{j} = j_0 e^{-i\omega t}$ Spin Hall	$\tilde{h} = h_0 e^{-i(\omega t - \Phi)}$ Field torque		$\tilde{j}_s = j_S e^{-i\omega t}$ Spin torque	Spin rectification[a,b]		Spin pumping[c]
dc voltage						$V \sim \langle Re(\tilde{j}) \cdot Re(\tilde{m}) \rangle$		$V \sim \lvert\tilde{h}\rvert^2$
Thin film	$\tilde{j} = \sigma\tilde{e}$		$\tilde{m} = \chi e^{i\Theta}\tilde{h}$			$V = V^{h}_{\mathrm{SR}} \cdot (e_0 h_0)$		
Bilayer	$\tilde{j} = \sigma\tilde{e}$	$\tilde{j}_s$	$\tilde{m} = \chi e^{i\Theta}\tilde{h}$	+	$\chi_j e^{i\vartheta}\tilde{j}_s$	$V = V^{h}_{\mathrm{SR}} \cdot (e_0 h_0) + V^{s}_{\mathrm{SR}} \cdot (j_0 j_S)$	+	$V_{\mathrm{SP}} \cdot h_0^2$
MTJ	$\tilde{j}, \tilde{j}_s$		$\tilde{m} = \chi e^{i\Theta}\tilde{h}$	+	$\chi_j e^{i\vartheta}\tilde{j}_s$	$V = V^{h}_{\mathrm{SR}} \cdot (e_0 h_0) + V^{s}_{\mathrm{SR}} \cdot (j_0 j_S)$		

[a] V^{h}_{SR}: Photovoltage caused by h-field torque induced *spin rectification* (including the so-called *AMR photovoltage*).[6,11–13,47]
[b] V^{s}_{SR}: Photovoltage caused by spin torque induced *spin rectification* (also known as the *spin diode effect*).[4,10,15,24]
[c] V_{SP}: Photovoltage caused by *spin pumping*.[7,8,19,20,25]

on a torque provided by the internal magnetic field $\mathbf{H}_i$ which acts on the magnetization $\mathbf{M}$, causing it to precess[53]

$$\frac{d\mathbf{M}}{dt} = -\gamma(\mathbf{M}\times\mathbf{H}_i) + \frac{\alpha}{M}\left(\mathbf{M}\times\frac{d\mathbf{M}}{dt}\right). \quad (1)$$

Here γ is the effective electron gyromagnetic ratio and α is the Gilbert damping parameter which can be used to determine the FMR linewidth ΔH in the linear regime, according to $\Delta H \sim \alpha\omega/\gamma$. For the case of microwave induced ferromagnetic resonance Eq. (1) can be solved by splitting the internal field into dc and rf components and taking the applied dc field $\mathbf{H}$ along the z axis. We can relate the internal field $\mathbf{H}_i = \mathbf{H}_{0i} + \mathbf{h}_i e^{-i\omega t}$ to the applied field through the demagnetization factors N_k, $H_{0iz} = H - N_z M_0$, $h_{ik} = h_k e^{i\Phi_k} - N_k m_k$, where Φ_k is the relative phase shift between the electric and magnetic fields in the kth direction and $\mathbf{M}_0$ is the dc magnetization also along the z axis. With the magnetization separated into dc and rf contributions $\mathbf{M} = \mathbf{M}_0 + \mathbf{m}e^{-i\omega t}$, the solution of Eq. (1) yields the dynamic susceptibility tensor $\widehat{\chi}$ which relates the magnetization $\mathbf{m}$ to the externally applied rf field $\mathbf{h}$,

$$\begin{aligned}\mathbf{m} = \widehat{\chi}\mathbf{h} &= \begin{pmatrix} \chi_{xx} & i\chi_{xy} & 0 \\ -i\chi_{xy} & \chi_{yy} & 0 \\ 0 & 0 & 0 \end{pmatrix}\mathbf{h} \\ &= \begin{pmatrix} |\chi_{xx}| & |\chi_{xy}|e^{i\frac{\pi}{2}} & 0 \\ |\chi_{xy}|e^{-i\frac{\pi}{2}} & |\chi_{yy}| & 0 \\ 0 & 0 & 0 \end{pmatrix}\mathbf{h}e^{i\Theta}, \end{aligned} \quad (2)$$

where $\Theta = \arctan[\Delta H/(H - H_r)]$ is the spin resonance phase[38] which describes the phase shift between the response and the driving force in terms of the linewidth ΔH and the resonance field H_r which are constant for a fixed frequency. Θ will change from 180° (driving force out of phase) to 0° (driving force in phase) around the resonance position, in a range on the order of ΔH, passing through 90° at resonance. This represents the universal feature of a resonance; the phase of the dynamic response always lags behind the driving force.[54]

To emphasize the resonant feature of the susceptibility tensor elements we define the symmetric Lorentz line shape L, and the dispersive line shape D as

$$\begin{aligned} L &= \frac{\Delta H^2}{(H - H_r)^2 + \Delta H^2}, \\ D &= \frac{\Delta H(H - H_r)}{(H - H_r)^2 + \Delta H^2}. \end{aligned} \quad (3)$$

Clearly the spin resonance phase can also be written in terms of L and D as $\Theta = \arctan[\Delta H/(H - H_r)] = \arctan(L/D)$ so that $L \propto \sin(\Theta)$ and $D \propto \cos(\Theta)$. Therefore L and D carry the resonant information of the susceptibility tensor.

Using L and D allows the elements of $\widehat{\chi}$ to be written as $(\chi_{xx}, \chi_{xy}, \chi_{yy}) = (D + iL)(A_{xx}, A_{xy}, A_{yy})$. A_{xx}, A_{xy} and A_{yy} are real amplitudes which are related to the sample properties

$$\begin{aligned} A_{xx} &= \frac{\gamma M_0[M_0 N_y + (H - N_z M_0)]}{\alpha\omega[2(H - N_z M_0) + M_0(N_z + N_y)]}, \\ A_{xy} &= -\frac{M_0}{\alpha[2(H - N_z M_0) + M_0(N_z + N_y)]}, \\ A_{yy} &= \frac{\gamma M_0[M_0 N_x + (H - N_z M_0)]}{\alpha\omega[2(H - N_z M_0) + M_0(N_z + N_y)]}. \end{aligned} \quad (4)$$

Since these amplitudes are real all components of $\widehat{\chi}$ include both a dispersive and a Lorentz line shape determined solely from the $D + iL$ term. However, in a transmission experiment performed using a resonance cavity $|m|^2 \propto L^2 + D^2 = L$ is measured. This product removes the phase dependence carried by L and D and leaves only the Lorentz line shape. For the same reason, the microwave photovoltage induced by spin pumping (the V_{SP} term in Table I) has a symmetric line shape.

The susceptibility for the two cases of in-plane and perpendicularly applied dc magnetic fields can easily be found from Eq. (4) by using the appropriate demagnetization factors. When the lateral dimensions are much larger than the thickness, $N_x = N_z = 0$ and $N_y = 1$ for an in-plane field and $N_x = N_y = 0$ and $N_z = 1$ for a field applied at a small angle from the perpendicular. In this paper we focus on the in-plane case. The line shape analysis for the perpendicular case can be found in Ref. 38. In both cases the form of the susceptibility $\chi \propto D + iL$ describes the ferromagnetic resonance line shape where each element of $\widehat{\chi}$ is the sum of an antisymmetric and symmetric Lorentz line shape. As we describe in the next section, via the V_{SR}^h term of the spin rectification effect, the symmetry properties of the dynamic susceptibility influence the symmetry of the electrically detected FMR which can be controlled by tuning the relative electromagnetic phase Φ.

C. Spin rectification induced by the field torque

The field-torque spin rectification effect results in the production of a dc voltage from the nonlinear coupling of rf electric and magnetic fields. For example, it may follow from the generalized Ohm's law[47,55]

$$\mathbf{J} = \sigma\mathbf{E}_0 - \frac{\sigma\Delta\rho}{\mathbf{M}^2}(\mathbf{J}\cdot\mathbf{M})\mathbf{M} + \sigma R_H \mathbf{J}\times\mathbf{M}, \quad (5)$$

where σ is the conductivity, $\Delta\rho$ is the resistivity change due to AMR, and R_H is the extraordinary Hall coefficient.

As shown in Fig. 2, we use two coordinate systems to describe a long narrow strip under the rotating in-plane magnetic field $\mathbf{H}$. The sample coordinate system $(\widehat{\mathbf{x}}', \widehat{\mathbf{y}}', \widehat{\mathbf{z}}')$ is fixed with the sample length along the z' direction and the sample width in the x' direction. The measurement coordinate system $(\widehat{\mathbf{x}}, \widehat{\mathbf{y}}, \widehat{\mathbf{z}})$ rotates with the $\mathbf{H}$ direction which is along the $\widehat{\mathbf{z}}$ axis. We define θ_H as the angle between the direction of the strip and the in-plane applied static magnetic field i.e., between the z' and z directions). In both coordinate systems, the $\widehat{\mathbf{y}}$ axis is along the normal of the sample plane. In the case of a sample length much larger than the width, the rf current $\tilde{j} = j_{z'}e^{-i\omega t}$ flows along the strip direction z'. In this geometry the field due to the Hall effect will only be in the transverse direction and will not generate a voltage along the strip. Taking the time average of the electric field integrated along the z' direction, the photovoltage is found as[11,12]

$$V = \frac{\Delta R}{M_0}\langle \mathrm{Re}(\tilde{j})\cdot\mathrm{Re}(\tilde{m}_x)\rangle \sin(2\theta_H), \quad (6)$$

where ΔR is the resistance change due to the AMR effect and the $\sin(2\theta_H)$ term is a result of the AMR effect which couples $\mathbf{J}$ and $\mathbf{M}$.

The susceptibility tensor given by Eqs. (2) and (4) can be used to write $\tilde{m}_x$ in terms of the rf $\mathbf{h}$ field. Since $\mathbf{M}_0$ and $\mathbf{H}$ are

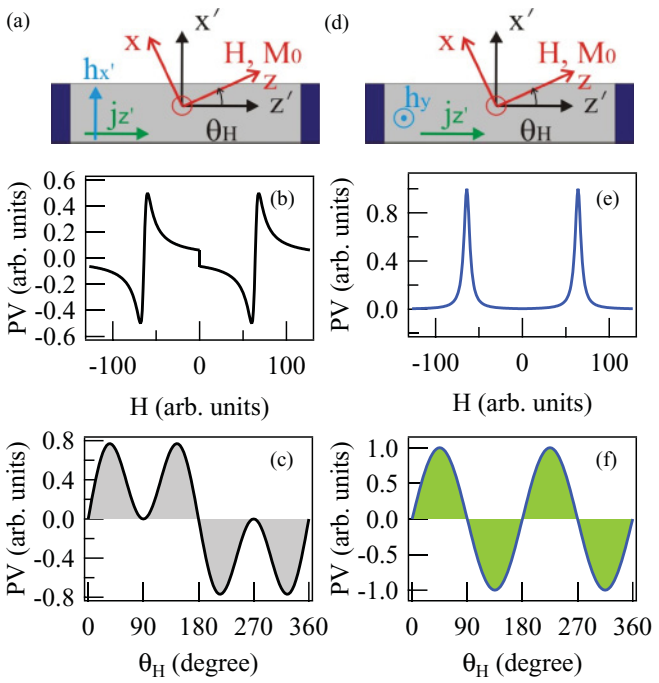

FIG. 2. (Color online) Left panel (a) Coordinate system for an in-plane dc H field applied along the z axis at an angle θ_H with respect to the z' axis, with a rf h field along the x' axis. (b) The calculated photovoltage (PV) spectrum at $\theta_H = 45^\circ$ and (c) the calculated amplitude of the PV spectrum at FMR as a function of θ_H according to Eq. (9). Right panel (d)–(f) are the same as (a)–(c), respectively, but with a rf h field along the y axis, and calculations are according to Eq. (10). In both cases, Φ is assumed to be zero for simplicity.

both along the z axis, only the components of **h** perpendicular to **z** will contribute to **m**. However, since the rf current flows in the z' direction, to calculate the rectified voltage, $\tilde{m}_x$ must be transformed into the (x', y, z') coordinate system by using the rotation $(\hat{\mathbf{x}}, \hat{\mathbf{y}}, \hat{\mathbf{z}}) = [\cos(\theta_H)\hat{\mathbf{x}}' - \sin(\theta_H)\hat{\mathbf{z}}', \hat{\mathbf{y}}, \sin(\theta_H)\hat{\mathbf{x}}' + \cos(\theta_H)\hat{\mathbf{z}}']$, which introduces an additional θ_H dependence into the photovoltage. We find that the photovoltage can be written in terms of the symmetric and antisymmetric Lorentz line shapes L and D as

$$V = \frac{\Delta R}{2M_0} j_{z'}(A_L L + A_D D), \tag{7}$$

where

$$\begin{aligned} A_L &= \sin(2\theta_H)[-A_{xx}h_{x'}\cos(\theta_H)\sin(\Phi_{x'}) \\ &\quad - A_{xy}h_y\cos(\Phi_y) + A_{xx}h_{z'}\sin(\theta_H)\sin(\Phi_{z'})], \\ A_D &= \sin(2\theta_H)[A_{xx}h_{x'}\cos(\theta_H)\cos(\Phi_{x'}) \\ &\quad - A_{xy}h_y\sin(\Phi_y) - A_{xx}h_{z'}\sin(\theta_H)\cos(\Phi_{z'})], \end{aligned} \tag{8}$$

and $\Phi_{x'}, \Phi_y$, and $\Phi_{z'}$ are the relative phases between electric and magnetic fields in the x', y, and z' directions, respectively.

The amplitudes of the Lorentz and dispersive line shape contributions show a complex dependence on the relative phases for the x', y, and z' directions and in general both line shapes will be present. However, depending on the experimental conditions, this dependence may be simplified. For instance, when $h_{x'}$ is the dominate driving field as shown in Fig. 2(a), we may take $h_y = h_{z'} \approx 0$ and $\Phi_{x'} = \Phi$, which results in

$$\begin{aligned} V = &-\frac{\Delta R}{2M_0} j_{z'} A_{xx} h_{x'} \cos(\theta_H)\sin(2\theta_H) \\ &\times [L\sin(\Phi) - D\cos(\Phi)]. \end{aligned} \tag{9}$$

From Eq. (9) we see that the photovoltage line shape changes from purely symmetric to purely antisymmetric in 90° intervals of Φ, being purely antisymmetric when $\Phi = n \times 180^\circ$ and purely symmetric when $\Phi = (2n+1) \times 90^\circ, n = 0, \pm 1, \pm 2 \ldots$.

As shown in Figs. 2(b) and 2(c), the photovoltage in Eq. (9) also shows symmetries depending on the static field direction θ_H. Since $\mathbf{H} \to -\mathbf{H}$ corresponds to $\theta_H \to \theta_H + 180^\circ$, $V(H) = -V(-H)$. Furthermore, at $\theta_H = n \times 90^\circ, n = 0, \pm 1, \pm 2, \ldots$ the voltage will be zero.

Similarly when h_y dominates as shown in Fig. 2(d), we take $h_{x'} = h_{z'} \approx 0$ and $\Phi_y = \Phi$ which results in a voltage

$$\begin{aligned} V = &-\frac{\Delta R}{2M_0} j_{z'} A_{xy} h_y \sin(2\theta_H) \\ &\times [L\cos(\Phi) + D\sin(\Phi)]. \end{aligned} \tag{10}$$

The symmetry properties are now such that the line shape is purely symmetric when $\Phi = n \times 180^\circ$ and purely antisymmetric when $\Phi = (2n+1) \times 90^\circ, n = 0, \pm 1, \pm 2 \ldots$. Also the photovoltage determined by Eq. (10) is now symmetric with respect to H under $\theta_H \to \theta_H + 180^\circ$ so that $V(H) = V(-H)$ as shown in Fig. 2(e). Therefore, experimentally the different symmetry of the FMR at H and $-H$ can be used as an indication of which component of the **h** field is dominant.

Both Eqs. (9) and (10) demonstrate that a change in the relative electromagnetic phase is expected to result in a change in the line shape of the electrically detected FMR. It is worth noting that when the relative phase $\Phi = 0$, the line shape is purely antisymmetric for FMR driven by $h_{x'}$ and purely symmetric for FMR driven by h_y as illustrated in Figs. 2(b) and 2(e), respectively. In the general case when $\tilde{m}_x$ is driven by multiple **h** components, Eq. (7) must be used in combination with angular (θ_H) dependent measurements in order to distinguish different contributions.

We also note that the above theoretical line shape analysis in the in-plane magnetic field case is consistent with our previous line shape study[38] in the perpendicular field case. In Ref. 38 we have established spintronic Michelson interferometry which enabled the demonstration of external control of the relative phase Φ. By applying such a novel technique, the measured response of the photovoltage line shape[38,39] was found to change its symmetry and polarity in 90° and 180° cycles of Φ, respectively, in excellent agreement with our line shape theory.

D. The physics of Φ

It is clear therefore that for field torque induced spin rectification, the relative phase Φ between the microwave electric and magnetic fields plays the pivotal role in the FMR line shape. Note that Φ is a material and frequency dependent property which is related to the losses in the system.[46,57,58] When a plane electromagnetic wave propagates through free space the electric and magnetic fields are in phase and orthogonal to each other.[56] However when the same electromagnetic

wave travels through a dispersive medium where the wave vector is complex, the imaginary contribution can create a phase shift between electric and magnetic fields. The most well known example is that of a plane electromagnetic wave moving in a conductor[46] where Faraday's law gives a simple relation between electric and magnetic fields $\omega\mu\mathbf{h} = \mathbf{k} \times \mathbf{e}$. Therefore the complex part of the wave vector $\mathbf{k}$ will induce a phase shift between electric and magnetic fields. Although the field will exponentially decay inside a conductor, it will still penetrate a distance on the order of the skin depth, and in a perfect conductor the conductivity, which produces an imaginary dielectric constant, will result in a phase shift of 45° between the electric and magnetic fields.[46]

In a complex system such as an experimental set up involving waveguides, coaxial cables, bonding wires, and a sample holder, which are required for electrical FMR detection, one cannot simply argue that Faraday's law itself is sufficient to explain the phase difference between the magnetic and electric field components. One needs to solve Maxwell's equations in their entirety by including full electromagnetic wave propagation with the relevant boundary conditions. The presence of electrical leads for measurement of dc voltage makes this problem very difficult. Nevertheless losses in the system which can be characterized in a variety of ways, such as through the wave impedance,[57,58] will lead to a phase shift between electric and magnetic fields which will influence the FMR line shape.

Although the physics of Φ is in principle contained in Maxwell's equations, due to the lack of technical tools for simultaneously and coherently probing both $\mathbf{e}$ and $\mathbf{h}$ fields, the effect of the relative phase had often been ignored until the recent development of spintronic Michelson interferometry.[38] In the following we provide systematically measured data showing the influence of the relative phase Φ on the line shape of FMR which is driven by different $\mathbf{h}$ field components.

IV. EXPERIMENTAL LINE SHAPE MEASUREMENTS

A. h_y dominant FMR

In order to use the h_y field to drive FMR a first generation spin dynamo was used where a Cu/Cr coplanar waveguide (CPW) was fabricated beside a Py microstrip with dimension 300 μm × 20 μm × 50 nm on a SiO_2/Si substrate as shown in Fig. 3(a). A microwave current is directly injected into the CPW and flows in the z' direction inducing a current in the Py strip also along the z' axis. In this geometry the dominant rf $\mathbf{h}$ field in the Py will be the Oersted field in the y direction produced according to Ampère's law. This field will induce FMR precession with the same cone angle independent of the in-plane orientation of the static field $\mathbf{H}$.

The AMR resistance depends on the orientation of the magnetization relative to the current and follows the relation $R(H) = R(0) - \Delta R \sin^2(\theta_M)$, where θ_M (not shown) is the angle between the magnetization and the current direction. For Py the AMR effect, which is responsible for the spin rectification, is observed to produce a resistance change of $\Delta R/R(0) \sim 0.4\%$. When $\mathbf{H}$ is applied along the x' axis, that is, the in-plane hard axis, the magnetization $\mathbf{M}$ tends to align toward the static field $\mathbf{H}$ and the angle θ_M is determined by $\sin(\theta_M) = H/H_A$ for $H < H_A$, where $H_A = N_{x'}M_0$ is the in-plane shape anisotropy field. The measured data (symbols) shown in Fig. 3(c) is fit (solid curve) according to $R(H) = R(0) - \Delta R \sin^2(\theta_M)$ with $R(0) = 112.66\Omega$, $\Delta R = 0.47\Omega$, $\mu_0 H_A = 4.0$ mT, and $N_{x'} = 0.004$.

Figure 3(d) shows that the line shape at $\theta_H = 120°$ and $\omega/2\pi = 5$ GHz is almost purely dispersive, indicating that at this frequency $\Phi \sim 90°$ according to Eq. (10). The θ_H dependence of H_r is shown in Fig. 3(e) and can be well fit by the function $\omega = \gamma\sqrt{[|H_r| + H_A\cos(2\theta_H)][|H_r| + M_0 - H_A(1 + \sin^2(\theta_H)]}$ by

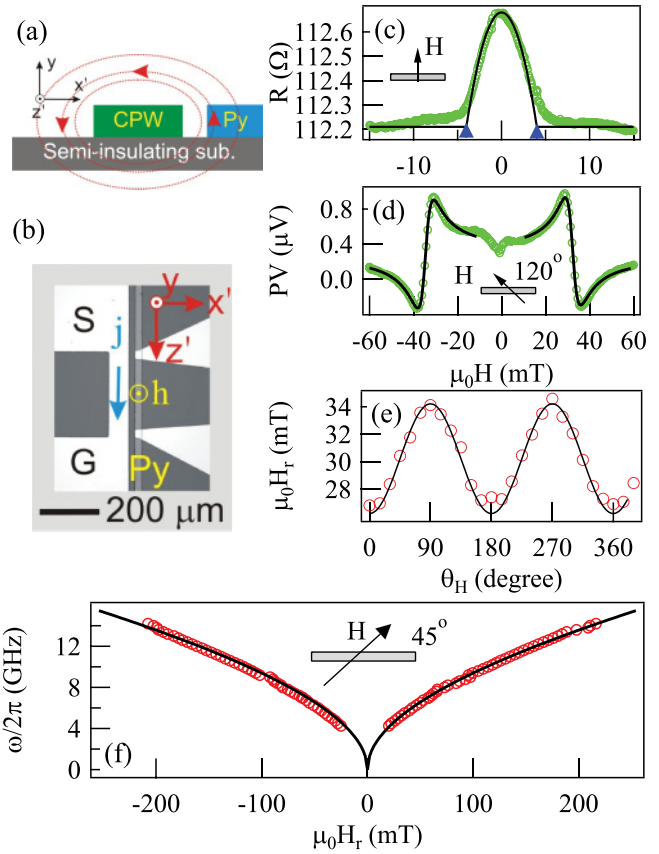

FIG. 3. (Color online) (a) Cross-sectional view of a schematic diagram showing the first generation spin dynamo where the Py strip is located beside the CPW. The dominate magnetic field in the Py is the Oersted field (indicated by circulating red arrows) in the y direction due to the current in the CPW. (b) Top view micrograph of the device showing the microwave current flowing in the shorted CPW and the direction of microwave h field on the Py strip. S and G denote the signal and ground line of the CPW, respectively. The Py microstrip is connected by two electrical leads in triangular shapes. (c) Magnetoresistance at $\theta_H = 90°$. AMR is seen to be ~0.4%. Arrows denote the anisotropic field $\mu_0 H_A = 4.0$ mT. Open circles are experimental data and solid curve is the fitting result using $R(0) = 112.66\Omega, \Delta R = 0.47\Omega, H_A = 4.0$ mT. (d) Electrically detected FMR at $\theta_H = 120°$ and $\omega/2\pi = 5$ GHz showing an almost purely dispersive line shape ($\Phi \simeq 90°$). Fit is according to Eq. (10) with $\mu_0\Delta H = 3.6$ mT, $\mu_0 H_r = 32.2$ mT. (e) Oscillating H_r dependence on the static field direction θ_H with amplitude $2H_A$. (f) Dependence of FMR frequency on the resonant field H_r at $\theta_H = 45°$. Open circles are experimental data and the solid line is the fit according to $\omega = \gamma\sqrt{|H_r|(|H_r| + M_0)}$.

taking the shape anisotropy field H_A along the x' axis into account.[59] As expected, the amplitude of these oscillations is $\mu_0 H_A = 4.0$ mT. The frequency dependence of H_r at $\theta_H = 45^\circ$ is shown in Fig. 3(f) and is fit using $\omega = \gamma\sqrt{|H_r|(|H_r| + M_0)}$ with $\gamma/2\pi = 29.0\mu_0$ GHz/T and $\mu_0 M_0 = 1.0$ T.

By systematically measuring the line shape as a function of the microwave frequency, we observe the interesting results of Fig. 4. The FMR line shape is observed to change from almost purely dispersive at $\omega/2\pi = 5$ GHz to almost purely symmetric at $\omega/2\pi = 5.56$ GHz. As discussed before, the line shape may be affected by the **h** orientation, that is, different **h** vector components will affect the line shape differently. Hence, if changing the microwave frequency changes the dominant driving field, the line shape may change. To rule out such a possibility an angular dependent experiment was performed to measure the line shape at different θ_H for each frequency ω. The results are plotted on the right panel of Fig. 4 which shows the sinusoidal curves for the Lorentz A_L and dispersive A_D amplitudes (dashed and solid curves, respectively) as a function of the static field angle θ_H. Both the Lorentz and dispersive amplitudes are found to follow a $\sin(2\theta_H)$ dependence on the field angle in agreement with Eq. (10) indicating that the magnetization precession is indeed dominantly driven by the h_y field. Therefore the line shape change indicates that the relative phase Φ is frequency dependent. As shown in Fig. 5(a), at $\omega/2\pi = 5$ GHz the amplitude of A_D is approximately one order of magnitude larger than A_L, while at $\omega/2\pi = 5.56$ GHz A_D is one order of magnitude less than A_L. Such a large change in A_L/A_D shows that in a microwave frequency range as narrow as 0.6 GHz, the relative phase Φ can change by 90°. Figure 5(b) shows Φ determined by using Eq. (10), which smoothly changes with microwave frequency except for a feature near 5.18 GHz, which is possibly caused by a resonant waveguide mode at this frequency.

Such a large change of Φ within a very narrow range of microwave frequency indicates the complexity of wave physics. Note that microwaves at ~5 GHz have wavelengths on the order of a few centimeters which are much larger than the submillimeter sample dimensions. Consequently, the microwave propagation depends strongly on the boundary conditions of Maxwell's equations which physically include the bonding wire, chip carrier, as well as the sample holder. This is similar to the microwave propagation in a waveguide where the field distribution, that is, the waveguide modes, are known to depend strongly on boundary conditions and frequency.[60] Despite the complex wave properties, the key message of our results is clear and consistent with the consideration of the physics of the relative phase: it shows

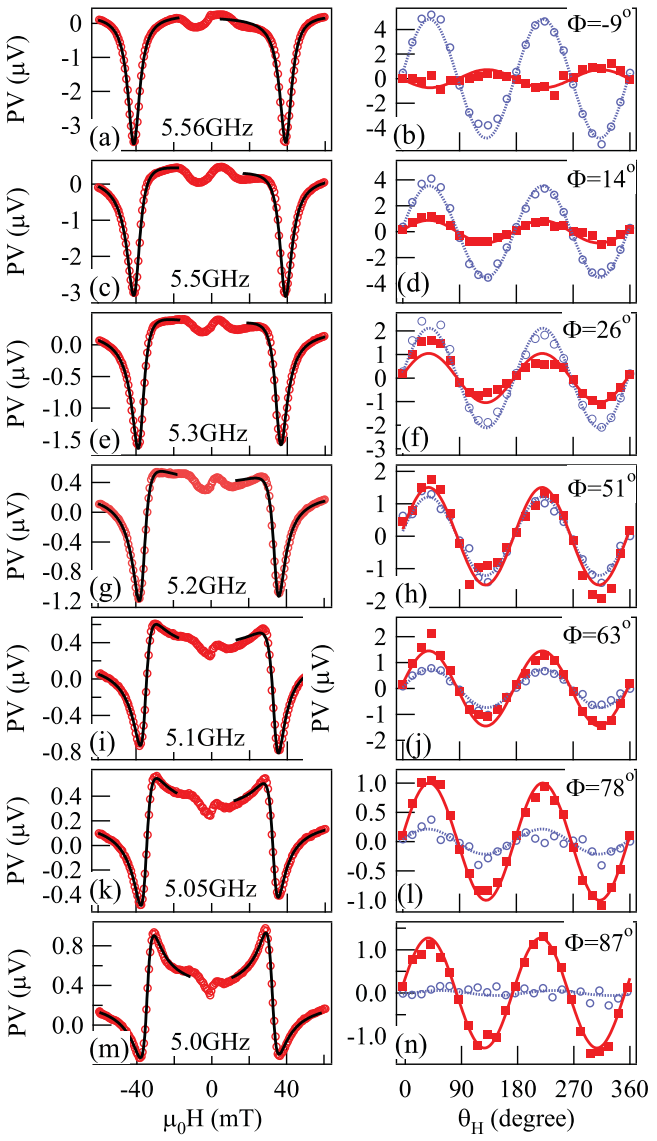

FIG. 4. (Color online) Data shown for a first generation spin dynamo. FMR spectra at $\theta_H = 120^\circ$ for several frequencies from 5.0 to 5.56 GHz with corresponding Lorentz and dispersive amplitudes as a function of θ_H. Circles and squares indicate the Lorentz and dispersive amplitudes of Eq. (10), respectively, and show a $\sin(2\theta_H)$ dependence as expected. Solid and dashed curves are $\sin(2\theta_H)$ functions.

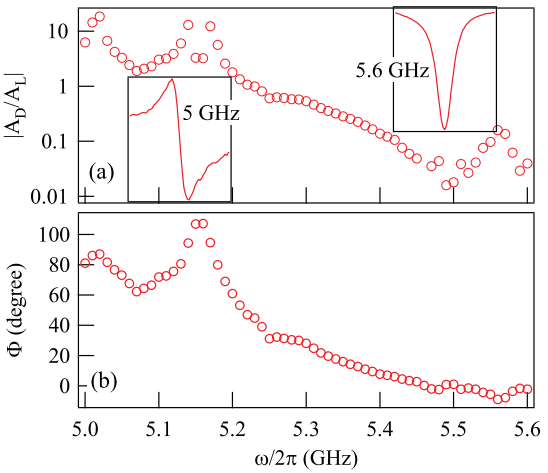

FIG. 5. (Color online) (a) The A_D/A_L ratio as a function of $\omega/2\pi$ showing the line shape change from dispersive at 5 GHz (left inset) to Lorentz at 5.6 GHz (right inset) with a step size of 0.01 GHz. (b) Φ dependence on $\omega/2\pi$ over same frequency interval showing the same dependence as A_D/A_L.

that in order to properly analyze the FMR line shape, Φ has to be determined for each frequency independently.

B. $h_{x'}$ dominant FMR

In order to drive the FMR using the rf field in the x' direction, $h_{x'}$, a second generation spin dynamo, was fabricated with the Py strip underneath the CPW as shown in Fig. 6. In this case the 300 μm $\times$ 7 μm $\times$ 100 nm Py strip is underneath the Cu/Cr coplanar waveguide which is fabricated on a SiO_2/Si substrate. Again a microwave current is directly injected into the CPW and induces a current in the z' direction in the Py strip. The dominant rf field in the Py is still the Oersted field, but due to the new geometry it is in the x' direction.

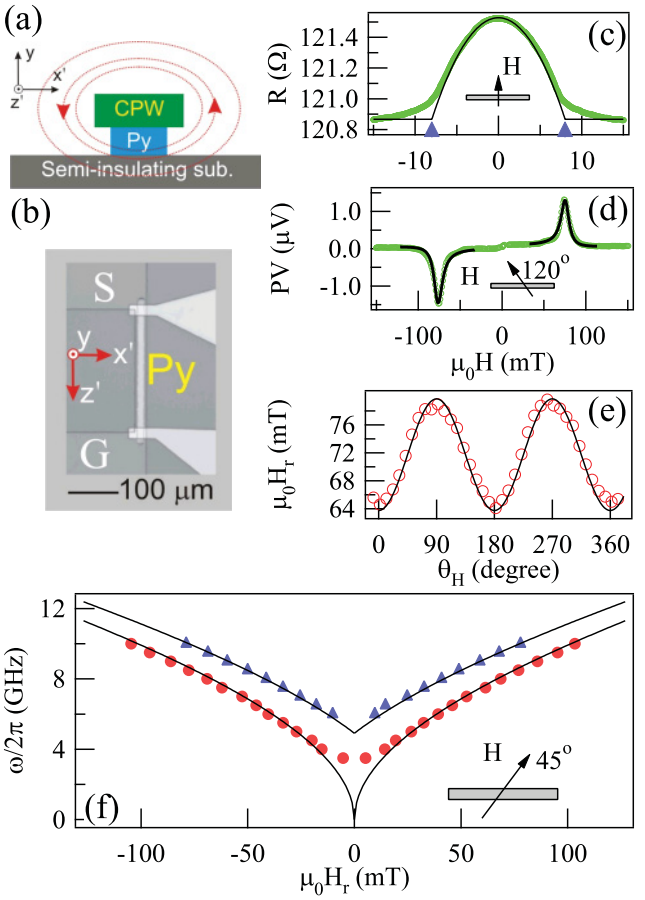

FIG. 6. (Color online) (a) Cross-sectional view of a schematic diagram showing the second generation spin dynamo where the Py strip is located underneath the CPW. In this case the dominant magnetic field in the Py is the Oersted field (indicated by circulating red arrows) in the x' direction due to the field in the CPW. (b) Top view micrograph of the Py microstrip underneath the shorted CPW (S and G denote the signal and ground line of the CPW, respectively). The Py microstrip is connected by two electrical leads in triangular shapes. (c) Magnetoresistance at $\theta_H = 90^\circ$. AMR is seen to be ~0.5%. Arrows denote the anisotropic field $\mu_0 H_A = 8.0$ mT. Open circles are experimental data and solid curve is the fitting result using $R(0) = 121.53\Omega$ and $\Delta R = 0.66\Omega$. (d) Electrically detected FMR at $\theta_H = 120^\circ$ and $\omega/2\pi = 8$ GHz showing a nearly symmetric Lorentz line shape. Fit is according to Eq. (10) with $\mu_0 \Delta H = 6.0$ mT, $\mu_0 H_r = 76.5$ mT, and $\Phi = -102^\circ$. (e) Oscillating H_r dependence on the static field direction θ_H with amplitude $2H_A$. (f) Dependence of FMR frequency on the resonant field H_r at $\theta_H = 45^\circ$. Solid circles show the FMR frequency dependence while the solid triangles are the standing SWR frequency dependence. The solid line is a fit to $\omega = \gamma\sqrt{|H_r|(|H_r| + M_0)}$.

Due to the smaller width and larger thickness, the demagnetization factor $N_{x'} = 0.008$ is twice that in the first generation sample. This corresponds to $\mu_0 H_A = 8.0$ mT as indicated by the broader AMR curve in Fig. 6(c). This value is further confirmed by the H_r vs θ_H plot shown in Fig. 6(e). Figure 6(f) shows the frequency dependence of H_r for FMR (circles) and for the first perpendicular standing spin wave resonance (SWR) (triangles) measured at $\theta_H = 45^\circ$. The frequency dependence of H_r follows $\omega = \gamma\sqrt{(|H_r| + H_{ex})(|H_r| + M_0 + H_{ex})}$ where H_{ex} is the exchange field. In Fig. 6(f) the standing SWR is fit using $\gamma/2\pi = 29.0\mu_0$ GHz/T, $\mu_0 H_{ex} = 30$ mT, and $\mu_0 M_0 = 1.0$ T.

Similar to the results presented in the previous section, the line shape of FMR measured on the second generation sample is also found to be frequency dependent (not shown). Hence, Φ is found to be nonzero in the general case. For example, at $\omega/2\pi = 8$ GHz, the line shape is found to be nearly symmetric, as shown in Fig. 6(d) for the FMR measured at $\theta_H = 120^\circ$, which indicates Φ is close to -90° at this frequency. Note that our result is in direct contrast with the recent study of Refs. 19 and 20, where experiments were measured in the same configuration and where it was suggested that $\Phi = 0^\circ$ for all samples at all frequencies.

While the line shape and hence the relative phase is found to be frequency dependent, Φ is expected to be independent of the static field direction θ_H. This is confirmed in Fig. 7(a) which shows the line shape measured at several values of θ_H in 10° increments. The data can be fit well using Eq. (9) with a constant $\Phi = -102^\circ$ for all θ_H. It confirms that the FMR is driven by a single **h** component, in this case the $h_{x'}$ field, and that Φ does not depend on θ_H. In Fig. 7(b) the θ_H dependence of A_L and A_D (solid/circles and dashed/squares, respectively) is shown. The circles and squares are experimental data while the solid and dashed lines are fitting results using a $\sin(2\theta_H)\cos(\theta_H)$ function according to Eq. (9). It provides further proof that the $h_{x'}$ field is responsible for driving the FMR in this sample.

While the results from both the first and second generation spin dynamos show consistently that Φ is sample and frequency dependent, the second generation spin dynamos exhibit special features in comparison with the first generation spin dynamos: the reduced separation between the Py strip and CPW enhances the $h_{x'}$ field so that the linewidth ΔH is enhanced by nonlinear magnetization damping,[27,28,61] which depends on the cone angle θ of the precession via the relation $\theta \sim h_{x'}\cos(\theta_H)/\Delta H(\theta)$. As shown in Fig. 7(c), ΔH is found to oscillate between 4.0 and 9.0 mT as θ_H changes. At $\theta_H = 0^\circ$, $\theta \sim h_{x'}/\Delta H$ and the cone angle is at its largest (about 4°). As θ_H increases from 0° and moves toward 90°, θ decreases so that the nonlinear damping contribution to ΔH decreases. Using the cone angle calculated from Fig. 7(c), we plot in Fig. 7(d) $\Delta H(\theta)$ as a function of the cone angle. It shows that ΔH has a quadratic dependence on the precession cone angle, which is in agreement with our previous study in the perpendicular **H**-field configuration.[27,28] We note that

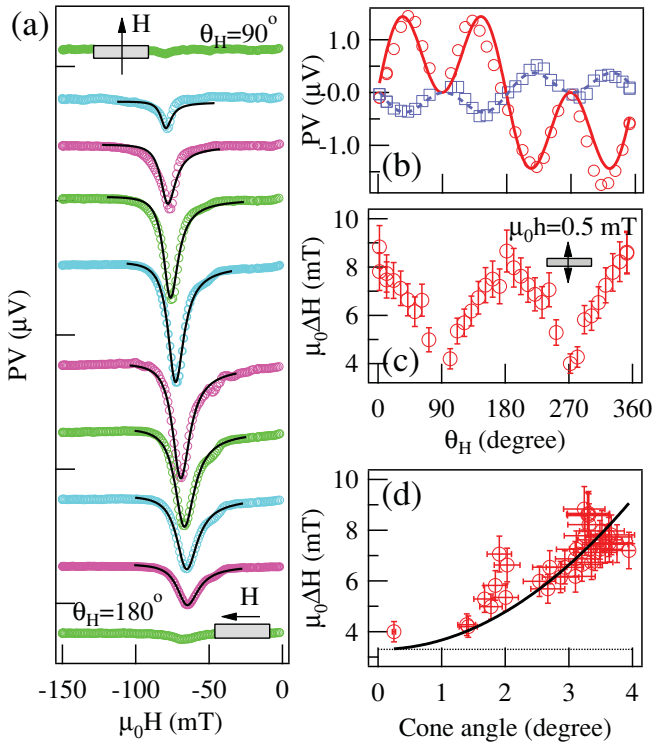

FIG. 7. (Color online) Data shown for a second generation spin dynamo. (a) FMR line shape at fixed frequency, $\omega/2\pi = 8$ GHz for several θ_H from 90° to 180° in steps of 10°. Open circles are experimental data and solid lines are fits using Eq. (9) with $\Phi = -102°$ fixed. (b) A_D and A_L shown in squares and circles respectively as a function of θ_H. Fitting curves are $\sin(2\theta_H)\cos(\theta_H)$ functions. (c) ΔH for several values of θ_H showing an oscillation with θ_H. (d) Nonlinear dependence of linewidth ΔH on the cone angle. Dashed line is the expected linear Gilbert damping whereas the data follows the quadratic dependence shown by the solid line.

for cone angles above only a few degrees, the nonlinear damping already dominates the contribution to ΔH. Hence, angular-dependent oscillations in the FMR linewidth provide a convenient way for verifying whether nonlinear effects may influence the electrically detected FMR.

C. Arbitrary *h* vector

Next we consider the most general case which is described by Eq. (7) where all components of **h** may contribute to the FMR line shape. The sample used here is a single Py strip where a waveguide with a horn antennae provided both the electric and magnetic driving fields. The sample chip is mounted near the center, at the end of a rectangular waveguide and the Py strip is directed along the short axis of the waveguide.

In a waveguide, the electromagnetic fields are well known and in general three components, $h_{x'}$,h_y, and $h_{z'}$ exist.[60] Figure 8(a) shows both the FMR and perpendicular standing SWR measured at $\theta_H = 45°$. Indeed both the amplitude and the line shape are different for the two FMR peaks located at H and $-H$, which indicates the existence of multiple **h** field components and Eqs. (7) and (8) are needed to separate them.

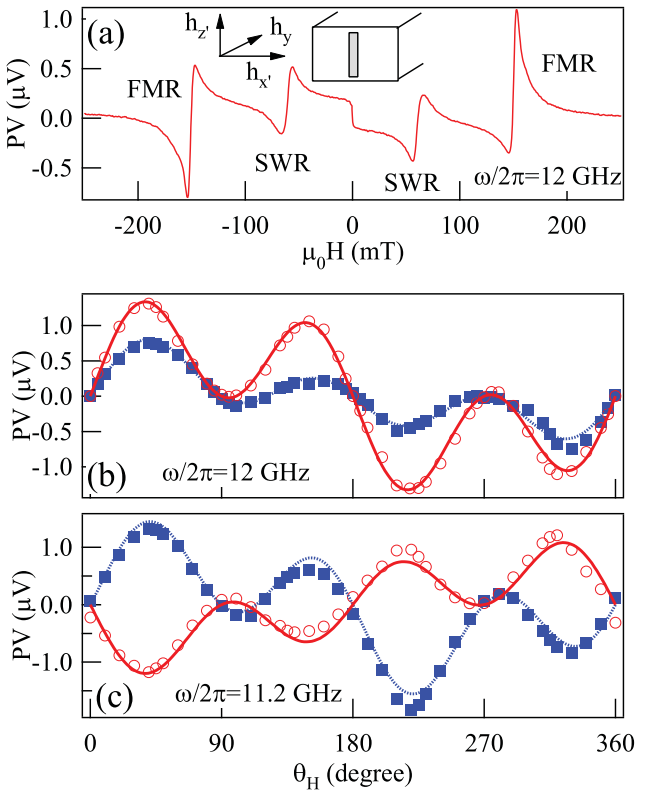

FIG. 8. (Color online) Data shown for a single Py strip with precession driven by horn antennae field. The strip dimensions are 3 mm × 50 μm × 45 nm. (a) Spectra showing distinct resonances due to FMR and SWR at $\omega/2\pi = 12$ GHz. (b) Separated Lorentz and dispersive line shapes (circles and squares, respectively) as a function of θ_H from a fit to Eq. (7) at $\omega/2\pi = 12$ GHz and (c) $\omega/2\pi = 11.2$ GHz.

This separation is done using the Lorentz and dispersive amplitudes determined from a fit to the FMR which are plotted as a function of θ_H in Figs. 8(b) and 8(c) for $\omega/2\pi = 12$ and 11.2 GHz, respectively. A fit using Eq. (8) allows a separation of the contributions from each of the $h_{x'}$,h_y, and $h_{z'}$ fields based on the their different contributions to the θ_H dependence of the line shape.

The results of the fit have been tabulated in Table II where $\gamma/2\pi = 28.0\mu_0$ GHz/T, $\mu_0 M_0 = 0.97$ T and $\mu_0 H_r = 152$ mT were used. The amplitudes of the different **h** field components have been normalized with respect to the $h_{x'}$ component. At both 11.2 and 12 GHz the $h_{x'}$ field is much larger than h_y or

TABLE II. Angular separation of **h** field components for 12 and 11.2 GHz.

	12 GHz	11.2 GHz
$\lvert h_{x'}\rvert$	1	1
$\lvert h_y\rvert$	0.02 ± 0.10	0.14 ± 0.07
$\lvert h_{z'}\rvert$	0.19 ± 0.06	0.37 ± 0.10
$\Phi_{x'}$	$-23 \pm 2°$	$50 \pm 2°$
Φ_y	$40 \pm 24°$	$-30 \pm 18°$
$\Phi_{z'}$	$-33 \pm 7°$	$82 \pm 5°$

$h_{z'}$, which is expected based on the wave propagation in a horn antennae.

We note that in this case with the device as long as 3 mm, the phase angle might change with position along the length of the device to an extent where a spread of angles should be taken into consideration. Nevertheless, even by using the crudest approximation to fit the data as if there is a single phase angle between each pair of e and h components, the relative phase for each component is seen to change significantly from 11.2 to 12 GHz. Therefore even in the case of a complex line shape produced by multiple **h** field components, by separating the individual contributions of the rf magnetic field via angular dependence measurements, the relative phase Φ of each field component is found to be frequency dependent.

D. Additional influences on Φ

In addition to the frequency and sample dependencies, the relative phase Φ may also depend on the lead configuration and wiring conditions of a particular device, as we have mentioned in Sec. IV A. Here we address such additional influences by using the first generation spin dynamos[11] shown in the inset of Fig. 9(a). Two spin dynamos with the same lateral dimensions but different Py thickness d are studied. Each spin dynamo involves two identical Py strips denoted by S1 and S2, one in each center of the G-S strips of the CPW, which are placed symmetrically with respect to the S strip. The current and rf **h** field are induced in the Py via a microwave current directly injected into the CPW. Similar to the sample discussed in Sec. IV A, h_y is the dominant field which drives the FMR.

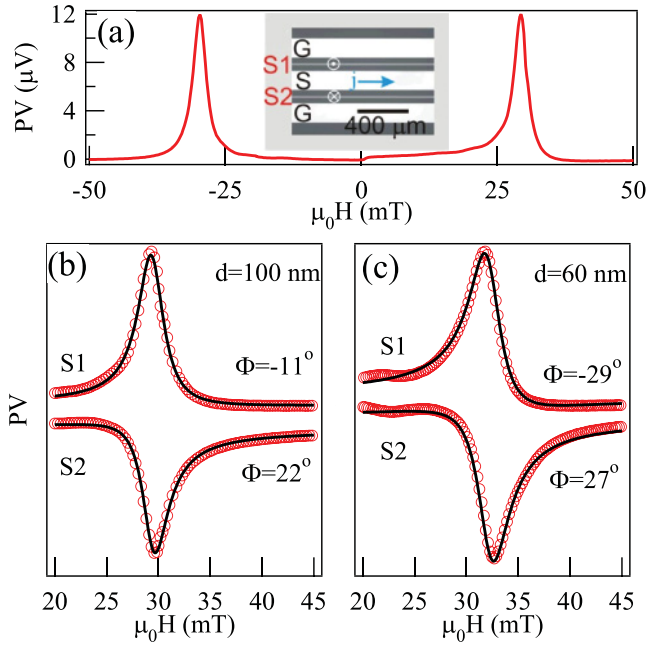

FIG. 9. (Color online) (a) FMR observed in a first generation spin dynamo. Inset shows the device structure with two Py strips labeled S1 and S2. (b) FMR for Py thickness $d = 100$ nm for both S1 and S2. In S1 $\Phi = -11^\circ$, while in S2 the line shape is slightly more asymmetric and $\Phi = 22^\circ$. (c) For $d = 60$ nm the relative phase is $\Phi = -29^\circ$ for S1 and $\Phi = 27^\circ$ for S2.

As shown in Fig. 9(a), FMR measured at $\omega/2\pi = 5$ GHz on the sample S1 with $d = 100$ nm shows a nearly symmetric Lorentz line shape and a field symmetry of $V(H) = V(-H)$. From the FMR line shape fitting, $\Phi = -11^\circ$ is found. Interestingly, as shown in Fig. 9(b), the FMR of the sample S2 of the same spin dynamo measured under the same experimental conditions shows a different line shape from which a different $\Phi = 22^\circ$ is found. We can further compare Φ measured on the other spin dynamo with a different Py thickness of $d = 60$ nm, also at $\omega/2\pi = 5$ GHz. Here for S1, $\Phi = -29^\circ$ while for S2, $\Phi = 27^\circ$. Again, the relative phase is found to be different for S1 and S2. These results demonstrate that due to additional influences such as different lead configuration and wiring conditions, even for samples with the same lateral dimensions Φ in each device is not necessarily the same. It demonstrates clearly that the relative phase Φ cannot be simply determined by analyzing the FMR line shape measured on a reference device. We note that our previous experiment performed using spintronic interferometry[38] also manifested similar sensitivity of the relative phase to the lead configuration and wiring conditions of a particular device.

E. Closing remarks

The experimental data presented above demonstrate the importance of the difference in the phase between the magnetic and electric field components and the role of the orientation of the rf magnetic field with respect to the film surface. Interpretation of the data depends on such a phase difference Φ, which is found to be sample and frequency dependent and nonzero in general. This nonzero phase results in both symmetric and antisymmetric Lorentz line shapes in the FMR detected via field-torque induced spin rectification. The Φ dependence of the line shape symmetry changes based on which component of the rf **h** field is responsible for driving the FMR precession. For instance a purely antisymmetric line shape could correspond to $\Phi = 0^\circ$ if the FMR is driven by $h_{x'}$, or to $\Phi = 90^\circ$ if the FMR is driven by h_y, therefore the line shape itself cannot be used to determine Φ directly. To separate the **h** field components an angular (θ_H) dependent measurement is necessary, which allows both **h** as well as the phase to be determined. Using such a measurement Φ has been observed to change from 0° to 90° in a narrow frequency range (0.6 GHz) resulting in a change from an antisymmetric to symmetric line shape demonstrating the large effect the relative phase has on the FMR line shape. Furthermore, Φ is not identical even in samples with the same geometric size. Therefore in our opinion, it is not a reliable approach to determine the pivotal relative phase Φ from different reference samples, as was adopted in some of the most recent studies.[19,20,24] Instead, to quantitatively interpret the measured microwave photovoltage induced by FMR, Φ should be calibrated for each sample, at each frequency, and for each measurement cycle.

V. Summary

We have provided a brief review of the rapidly growing literature on electrical detection of spin dynamics in micro- and nanodevices. We have focused on the important issue of

the relation and distinction between different mechanisms that give rise to the rf photovoltage via FMR in spintronic devices. Such a photovoltage has in general two different types of origins: spin pumping (V_{SP}) and spin rectification (V_{SR}), where the spin rectification may be induced by either rf h field or spin torque, which give rise to the photovoltages V_{SR}^{h} and V_{SR}^{s}, respectively.

We have shown that in order to distinguish different mechanisms which enable the electrical detection of FMR via microwave photovoltages, it is essential to properly analyze the FMR line shape. While spin pumping is an incoherent and interfacial effect which always gives rise to a symmetric FMR line shape in V_{SP}, spin rectification is not restricted at the interface and is caused by coherent coupling between rf current and magnetization. Hence, the FMR line shape of V_{SR} is intriguingly phase dependent and may have both symmetric and antisymmetric components. We have found theoretically that for rf h-field torque induced spin rectification, the FMR line shape of V_{SR}^{h} depends strongly on the relative phase Φ between the rf e and h fields used to drive the current and magnetization, respectively. Analytical formulas have been established to analyze the FMR line shape of V_{SR}^{h}, and our approach based on the dynamic susceptibility can be further generalized to analyze the FMR line shape of spin torque induced photovoltage V_{SR}^{s}.

Based on a systematic study of the measured photovoltage, the FMR line shape of V_{SR}^{h} is observed to depend strongly on the microwave frequency, driving field configuration, sample structure, and even wiring conditions. Therefore we have presented strong evidence that within the standard microwave circuit geometries used to build spintronic devices, it is common for nonzero relative phase Φ to exist at the spin device location. This could cause a skew in the field-swept FMR line shape which, when this phase angle is unknown, can lead to unintentional quantitative errors when extracting individual mechanistic contributions to the photovoltage by fitting the line shapes. Our results imply that for electrically detected FMR which involves both spin Hall and spin rectification effects, the pivotal relative phase must be either directly calibrated or precisely controlled in order to properly analyze the FMR line shape and quantify the spin Hall angle. For such studies, we strongly suggest not to use the unreliable approach of determining Φ from reference samples, but instead recommend applying spintronic Michelson interferometry[38] which enables external control of the relative phase.

ACKNOWLEDGMENTS

We would like to thank B. W. Southern, A. Hoffmann, S. D. Bader, B. Heinrich, D. C. Ralph, G. E. W. Bauer, and S.M. Rezende for discussions. This work has been funded by NSERC, CFI, CMC, and URGP grants (C.-M.H.). Z.X.C. was supported by the National Natural Science Foundation of China Grant No. 10990100.

*hu@physics.umanitoba.ca; URL: http://www.physics.umanitoba.ca/∼hu

[1] M. Tsoi, A. G. M. Jansen, J. Bass, W.-C. Chiang, V. Tsoi, and P. Wyder, Nature (London) **406**, 46 (2000).

[2] S. I. Kiselev, J. C. Sankey, I. N. Krivorotov, N. C. Emley, R. J. Schoelkopf, R. A. Buhrman, and D. C. Ralph, Nature (London) **425**, 380 (2003).

[3] Y. S. Gui, S. Holland, N. Mecking, and C.-M. Hu, Phys. Rev. Lett. **95**, 056807 (2005).

[4] A. A. Tulapurkar, Y. Suzuki, A. Fukushima, H. Kubota, H. Maehara, K. Tsunekawa, D. D. Djayaprawira, N. Watanabe, and S. Yuasa, Nature (London) **438**, 339 (2005).

[5] A. Azevedo, L. H. Vilela Leo, R. L. Rodriguez-Suarez, A. B. Oliveira, and S. M. Rezende, J. Appl. Phys. **97**, 10C715 (2005).

[6] M. V. Costache, S. M. Watts, M. Sladkov, C. H. van der Wal, and B. J. van Wees, Appl. Phys. Lett. **89**, 232115 (2006).

[7] M. V. Costache, M. Sladkov, S. M. Watts, C. H. van der Wal, and B. J. van Wees, Phys. Rev. Lett. **97**, 216603 (2006).

[8] E. Saitoh, M. Ueda, H. Miyajima, and G. Tatara, Appl. Phys. Lett. **88**, 182509 (2006).

[9] J. C. Sankey, P. M. Braganca, A. G. F. Garcia, I. N. Krivorotov, R. A. Buhrman, and D. C. Ralph, Phys. Rev. Lett. **96**, 227601 (2006).

[10] H. Kubota, A. Fukushima, K. Yakushiji, T. Nagahama, S. Yuasa, K. Ando, H. Maehara, Y. Nagamine, K. Tsunekawa, D. D. Djayaprawira, N. Watanabe, and Y. Suzuki, Nat. Phys. **4**, 37 (2007).

[11] Y. S. Gui, N. Mecking, X. Zhou, G. Williams, and C. -M. Hu, Phys. Rev. Lett. **98**, 107602 (2007).

[12] N. Mecking, Y. S. Gui, and C.-M. Hu, Phys. Rev. B **76**, 224430 (2007).

[13] A. Yamaguchi, H. Miyajima, T. Ono, Y. Suzuki, S. Yuasa, A. Tulapurkar, and Y. Nakatani, Appl. Phys. Lett. **90**, 182507 (2007).

[14] S. T. Goennenwein, S. W. Schink, A. Brandlmaier, A. Boger, M. Opel, R. Gross, R. S. Keizer, T. M. Klapwijk, A. Gupta, H. Huebl, C. Bihler, and M. S. Brandt, Appl. Phys. Lett. **90**, 162507 (2007).

[15] J. C. Sankey, Y. T. Cui, J. Z. Sun, J. C. Slonczewski, Robert A. Buhrman, and D. C. Ralph, Nat. Phys. **4**, 67 (2008).

[16] X. Hui, A. Wirthmann, Y. S. Gui, Y. Tian, X. F. Jin, Z. H. Chen, S. C. Shen, and C. -M. Hu, Appl. Phys. Lett. **93**, 232502 (2008).

[17] A. Wirthmann, X. Hui, N. Mecking, Y. S. Gui, T. Chakraborty, C. -M. Hu, M. Reinwald, C. Schüller, and W. Wegscheider, Appl. Phys. Lett. **92**, 232106 (2008).

[18] V. A. Atsarkin, V. V. Demidov, L. V. Levkin, and A. M. Petrzhik, Phys. Rev. B **82**, 144414 (2010).

[19] O. Mosendz, J. E. Pearson, F. Y. Fradin, G. E. W. Bauer, S. D. Bader, and A. Hoffmann, Phys. Rev. Lett. **104**, 046601 (2010).

[20] O. Mosendz, V. Vlaminck, J. E. Pearson, F. Y. Fradin, G. E. W. Bauer, S. D. Bader, and A. Hoffmann, Phys. Rev. B **82**, 214403 (2010).

[21] P. Saraiva, A. Nogaret, J. C. Portal, H. E. Beere, and D. A. Ritchie, Phys. Rev. B **82**, 224417 (2010).

[22] Y. Kajiwara, K. Harii, S. Takahashi, J. Ohe, K. Uchida, M. Mizuguchi, H. Umezawa, H. Kawai, K. Ando, K. Takanashi, S. Maekawa, and E. Saitoh, Nature (London) **464**, 262 (2010).

[23]C. W. Sandweg, Y. Kajiwara, K. Ando, E. Saitoh, and B. Hillebrands, Appl. Phys. Lett. **97**, 252504 (2010).
[24]L. Liu, T. Moriyama, D. C. Ralph, and R. A. Buhrman, Phys. Rev. Lett. **106**, 036601 (2011).
[25]A. Azevedo, L. H. Vilela Leão, R. L. Rodríguez-Suárez, A. F. Lacerda Santos, and S. M. Rezende, Phys. Rev. B **83**, 144402 (2011).
[26]Y. S. Gui, N. Mecking, and C.-M. Hu, Phys. Rev. Lett. **98**, 217603 (2007).
[27]Y. S. Gui, A. Wirthmann, N. Mecking, and C.-M. Hu, Phys. Rev. B **80**, 060402(R) (2009).
[28]Y. S. Gui, A. Wirthmann, and C.-M. Hu, Phys. Rev. B **80**, 184422 (2009).
[29]C. T. Boone, J. A. Katine, J. R. Childress, V. Tiberkevich, A. Slavin, J. Zhu, X. Cheng, and I. N. Krivorotov, Phys. Rev. Lett. **103**, 167601 (2009).
[30]D. Bedau, M. Kläui, S. Krzyk, U. Rüdiger, G. Faini, and L. Vila, Phys. Rev. Lett. **99**, 146601 (2007).
[31]S. Bonetti, V. Tiberkevich, G. Consolo, G. Finocchio, P. Muduli, F. Mancoff, A. Slavin, and J. Åkerman, Phys. Rev. Lett. **105**, 217204 (2010).
[32]S. Urazhdin, V. Tiberkevich, and A. Slavin, Phys. Rev. Lett. **105**, 237204 (2010).
[33]Y. Tserkovnyak, A. Brataas, G. E. W. Bauer, and B. I. Halperin, Rev. Mod. Phys. **77**, 1375 (2005).
[34]L. Berger, Phys. Rev. B **59**, 11465 (1999).
[35]A. Brataas, Y. Tserkovnyak, G. E. W. Bauer, and B. I. Halperin, Phys. Rev. B **66**, 060404 (2002).
[36]X. Wang, G. E. W. Bauer, B. J. van Wees, A. Brataas, and Y. Tserkovnyak, Phys. Rev. Lett. **97**, 216602 (2006).
[37]A. Yamaguchi, H. Miyajima, S. Kasai, and T. Ono, Appl. Phys. Lett. **90**, 212505 (2007).
[38]A. Wirthmann, X. Fan, Y. S. Gui, K. Martens, G. Williams, J. Dietrich, G. E. Bridges, and C.-M. Hu, Phys. Rev. Lett. **105**, 017202 (2010).
[39]X. F. Zhu, M. Harder, A. Wirthmann, B. Zhang, W. Lu, Y. S. Gui, and C.-M. Hu, Phys. Rev. B **83**, 104407 (2011).
[40]X. Fan, S. Kim, X. Kou, J. Kolodzey, H. Zhang, and J. Q. Xiao, Appl. Phys. Lett. **97**, 212501 (2010).
[41]L. H. Bai, Y. S. Gui, A. Wirthmann, E. Recksiedler, N. Mecking, C.-M. Hu, Z. H. Chen, and S. C. Shen, Appl. Phys. Lett. **92**, 032504 (2008).
[42]H. Zhao, E. J. Loren, H. M. van Driel, and A. L. Smirl, Phys. Rev. Lett. **96**, 246601 (2006).
[43]J. Wang, B. F. Zhu, and R. B. Liu, Phys. Rev. Lett. **104**, 256601 (2010).
[44]L. K. Werake and H. Zhao, Nat. Phys. **6**, 875 (2010).
[45]Via private communications, Dr. Hoffmann suggests that "The fact of the matter is that the experiments (Refs. 19 and 24) are conceptually very different and also in their approach very different. In the Cornell experiment (Ref. 24) the rf current is applied directly to the Py/Pt bilayer, while in our case (Ref. 19) only a small fraction of the rf current flows through the bilayer as a consequence of the capacitive coupling. This means that in the Cornell measurement the ratio of rf current to the rf magnetic field exciting the magnetization dynamics is significantly higher than in our experiments and that is the reason why the ratio of any voltages from spin Hall effects compared to AMR voltages is significantly smaller than in our experiments." We note that it is an important task to check whether such an interesting interpretation might be directly confirmed in a controlled experiment, for example, by directly comparing the photovoltage measured on the same Py/Pt bilayer using two different approaches for applying the rf current.
[46]J. D. Jackson, *Classical Electrodynamics*, 2nd ed. (John Wiley & Sons, New York, 1975).
[47]H. J. Juretschke, J. Appl. Phys. **31**, 1401 (1960).
[48]R. H. Silsbee, A. Janossy, and P. Monod, Phys. Rev. B **19**, 4382 (1979).
[49]B. Heinrich, Y. Tserkovnyak, G. Woltersdorf, A. Brataas, R. Urban, and G. E. W. Bauer, Phys. Rev. Lett. **90**, 187601 (2003).
[50]J. N. Kupferschmidt, S. Adam, and P. W. Brouwer, Phys. Rev. B **74**, 134416 (2006).
[51]A. A. Kovalev, G. E. W. Bauer, and A. Brataas, Phys. Rev. B **75**, 014430 (2007).
[52]Via private communications, Dr. Rezende points out that their group, unaware of Ref. 38, has worked independently on the question of the line shape and developed a theory (Ref. 25) for V_{SR}^{h} that considered both Lorentzian and dispersive components which are essential to fit their data for the angular dependence of the dc voltage produced by FMR. Specifically, Dr. Rezende points out that they have the following independent findings: (1) The important role and the consequence of the phase between the external rf h field and the induced rf current, which was previously considered to be 0° (or 90° depending on reference). (2) The existence of the Lorentzian component of V_{SR}^{h}. Previous papers (Refs. 19 and 20) considered that V_{SR}^{h} had only a Lorentzian derivative component and that, as they have pointed out in their paper (Ref. 25), was one of the reasons for the erroneous values for the material parameters obtained previously.
[53]T. L. Gilbert, IEEE Trans. Magn. **40**, 3443 (2004).
[54]L. D. Landau and E. M. Lifshitz, *Mechanics*, 2nd ed. (Pergamon, Oxford, 1969).
[55]J. P. Jan, in *Solid State Physics*, edited by F. Seitz and D. Turnbull (Academic, New York, 1957), Vol. 5.
[56]M. Born and E. Wolf, *Principles of Optics: Electromagnetic Theory of Propagation, Interference and Diffraction*, 7th ed. (Cambridge University Press, Cambridge, 1999).
[57]W. Heinrich, IEEE Trans. Microwave Theory Tech. **38**, 1468 (1990).
[58]W. Heinrich, IEEE Trans. Microwave Theory Tech. **41**, 45 (1993).
[59]S. V. Vonsovskii, *Ferromagnetic Resonance: The Phenomenon of Resonant Absorption of a High-Frequency Magnetic Field in Ferromagnetic Substances*, (Pergamon, Oxford, 1966).
[60]B. S. Guru and H. R. Hiziroglu, *Electromagnetic Field Theory Fundamentals*, 2nd ed. (Cambridge University Press, Cambridge, 2004).
[61]V. Tiberkevich and A. Slavin, Phys. Rev. B **75**, 014440 (2007).